ISSN 1674-1056
http://cpb.iphy.ac.cn
http://iopscience.iop.org/cpb
中国物理 B
Chinese Physics
中国物理 Chinese Physics B

Ab initio calculations on oxygen vacancy defects in strained amorphous silica

Bao-Hua Zhou(周保花), Fu-Jie Zhang(张福杰), Xiao Liu(刘笑), Yu Song(宋宇), Xu Zuo(左旭)

Citation: Chin. Phys. B . 2020, 29(4): 047103 . **doi:** 10.1088/1674-1056/ab75db
Journal homepage: http://cpb.iphy.ac.cn; http://iopscience.iop.org/cpb

What follows is a list of articles you may be interested in

Electronic properties of size-dependent $MoTe_2$/WTe_2 heterostructure

Jing Liu(刘婧), Ya-Qiang Ma(马亚强), Ya-Wei Dai(戴雅薇), Yang Chen(陈炀), Yi Li(李依), Ya-Nan Tang(唐亚楠), Xian-Qi Dai(戴宪起)

Chin. Phys. B . 2019, 28(10): 107101 . **doi:** 10.1088/1674-1056/ab3b53

Prediction of high-mobility two-dimensional electron gas at $KTaO_3$-based heterointerfaces

Fu-Ning Wang(王芙凝), Ji-Chao Li(李吉超), Yi Li(李宜), Xin-Miao Zhang(张鑫淼), Xue-Jin Wang(王学晋), Yu-Fei Chen(陈宇飞), Jian Liu(刘剑), Chun-Lei Wang(王春雷), Ming-Lei Zhao(赵明磊), Liang-Mo Mei(梅良模)

Chin. Phys. B . 2019, 28(4): 047101 . **doi:** 10.1088/1674-1056/28/4/047101

Graphene-like Be_3X_2 (X=C, Si, Ge, Sn): A new family of two-dimensional topological insulators

Lingling Song(宋玲玲), Lizhi Zhang(张礼智), Yurou Guan(官雨柔), Jianchen Lu(卢建臣), Cuixia Yan(闫翠霞), Jinming Cai(蔡金明)

Chin. Phys. B . 2019, 28(3): 037101 . **doi:** 10.1088/1674-1056/28/3/037101

Exploration of the structural and optical properties of a red-emitting phosphor $K_2TiF_6:Mn^{4+}$

Xi-Long Dou(豆喜龙), Xiao-Yu Kuang(邝小渝), Xin-Xin Xia(夏欣欣), Meng Ju(巨濛)

Chin. Phys. B . 2019, 28(1): 017107 . **doi:** 10.1088/1674-1056/28/1/017107

Antiferromagnetic–ferromagnetic transition in zigzag graphene nanoribbons induced by substitutional doping

Shenyuan Yang(杨身园), Jing Li(李静), Shu-Shen Li(李树深)

Chin. Phys. B . 2018, 27(11): 117102 . **doi:** 10.1088/1674-1056/27/11/117102

Ab initio calculations on oxygen vacancy defects in strained amorphous silica*

Bao-Hua Zhou(周保花)[1,†], Fu-Jie Zhang(张福杰)[1], Xiao Liu(刘笑)[1], Yu Song(宋宇)[2,3], and Xu Zuo(左旭)[1,4,‡]

[1] *College of Electronic Information and Optical Engineering, Nankai University, Tianjin* 300071, *China*
[2] *Microsystem and Terahertz Research Center, China Academy of Engineering Physics, Chengdu* 610200, *China*
[3] *Institute of Electronic Engineering, China Academy of Engineering Physics, Mianyang* 621999, *China*
[4] *Key Laboratory of Photoelectronic Thin Film Devices and Technology of Tianjin, Tianjin* 300350, *China*

(Received 22 January 2020; revised manuscript received 9 February 2020; accepted manuscript online 13 February 2020)

The effects of uniaxial tensile strain on the structural and electronic properties of positively charged oxygen vacancy defects in amorphous silica (a-SiO_2) are systematically investigated using *ab-initio* calculation based on density functional theory. Four types of positively charged oxygen vacancy defects, namely the dimer, unpuckered, and puckered four-fold (4×), and puckered five-fold (5×) configurations have been investigated. It is shown by the calculations that applying uniaxial tensile strain can lead to irreversible transitions of defect structures, which can be identified from the fluctuations of the curves of relative total energy versus strain. Driven by strain, a positively charged dimer configuration may relax into a puckered 5× configuration, and an unpuckered configuration may relax into either a puckered 4× configuration or a forward-oriented configuration. Accordingly, the Fermi contacts of the defects remarkably increase and the defect levels shift under strain. The Fermi contacts of the puckered configurations also increase under strain to the values close to that of E'_α center in a-SiO_2. In addition, it is shown by the calculations that the relaxation channels of the puckered configurations after electron recombination are sensitive to strain, that is, those configurations are more likely to relax into a two-fold coordinated Si structure or to hold a puckered structure under strain, both of which may raise up the thermodynamic charge-state transition levels of the defects into Si band gap. As strain induces more puckered configurations with the transition levels in Si band gap, it may facilitate directly the development of oxide charge accumulation and indirectly that of interface charge accumulation by promoting proton generation under ionization radiation. This work sheds a light on understanding the strain effect on ionization damage at an atomic scale.

Keywords: amorphous silica, first-principles calculation, strain, oxygen vacancy defects

PACS: 71.15.Mb, 71.20.–b, 61.72.Hh, 61.80.Az **DOI:** 10.1088/1674-1056/ab75db

1. Introduction

Amorphous silica (a-SiO_2) is the most widely-used dielectric insulator in semiconductor devices. It can be conveniently grown in relatively high quality by thermal oxidation on top of silicon, which made a-SiO_2 the most common gate dielectric in metal-oxide-semiconductor (MOS) devices. Even though the gate dielectrics have evolved to be high-*k* dielectrics in high-speed logic devices, a-SiO_2 still dominates the power devices that require a thick gate dielectric and fast oxidation in fabrication. The amorphous nature of a-SiO_2 implies a relative high concentration of point defects, especially neutral oxygen vacancies (NOVs), which may make the semiconductor devices using a-SiO_2 dielectric sensitive to certain extreme environments and result in reliability issues. In space applications, for example, an NOV and its charged derivatives can participate in several critical processes and reactions that ultimately lead to ionization damage of devices.[1] In addition, the reactions involved in ionization damage are coupled with each other, and jointly result in the puzzling enhanced low-dose-rate sensitivity (ELDRS),[2–4] by which the damage is counterintuitively more severe at low dose rate. More than that, it was demonstrated by experiments that the strain induced by the passivation layer of the devices was able to influence ELDRS.[5,6] It is thus possible to inhibit ELDRS by a careful choice of passivation material and processing, in the step of encapsulation.[7] However, the atomic-scale mechanism behind this effect is totally unknown. It can only be suspected that the strain induced by the passivation layer may impact the oxide defects and then influence ELDRS indirectly. Therefore, it is of great interest, in both theory and application, to study the defect properties in strained a-SiO_2.

Defects in a-SiO_2 play a key role in ionization damage, contributing to both oxide and interface charge accumulations that affect device operation. Oxygen vacancy defects, as the most common intrinsic defects in a-SiO_2, have attracted extensive attention in the past decades. Blöchl studied the oxygen vacancy defects in a-SiO_2 using *ab initio* calculations.[8] It was found that an NOV can convert into a dimer or puck-

*Project supported by the Science Challenge Project, China (Grant No. TZ2016003-1-105) and the CAEP Microsystem and THz Science and Technology Foundation (Grant No. CAT201501).

†Corresponding author. E-mail: z_baohua@126.com
‡Corresponding author. E-mail: xzuo@nankai.edu.cn; xzuonku@qq.com

© 2020 Chinese Physical Society and IOP Publishing Ltd

ered configuration after trapping a hole, which is associated with the E'_δ or E'_γ center detected in the electron paramagnetic resonance (EPR) spectrum. The thermodynamic charge-state transition levels of E'_δ and E'_γ centers were calculated. The levels of E'_δ centers were above the a-SiO_2 valence band maximum (VBM) and below the Si VBM, and those of E'_γ centers were in the middle of Si band gap. It was then deduced that E'_δ center is thermodynamically unstable for the Fermi level of a normal device that is generally in Si bandgap, and that E'_γ center is thermodynamically stable. Thus, the contribution to oxide charge accumulation is mainly from puckered configurations.[9] In addition, thermodynamic charge-state transition level depends on the relaxed structures after capturing a hole and then an electron. Uchino studied and summarized the possible relaxation channels of NOVs after hole capture and electron recombination.[10] After capturing a hole, an NOV may relax into the positively-charged configurations with different structures, namely dimer, puckered, and forward-oriented (FO) structures. When the positively-charged configurations are neutralized by re-capturing an electron, they may relax into different neutral structures. The dimer configuration maintains the structure but with a shorter Si–Si bond length. The puckered configuration collapses into the dimer structure in neutral. The FO configuration converts into a divalent silicon structure. In addition, it has been shown by the first-principles calculations that the Si atom can be five-fold coordinated in a puckered configuration besides being four-fold coordinated.[11] After capturing an electron, some instances of the puckered four-fold coordinated ($4\times$) configurations can hold the structure, and the electron resides on the dangling bond orbit, which results in an electric dipole across the defect. On the contrary, the positively charged puckered five-fold coordinated ($5\times$) configurations all collapse into the neutral dimer structure.

The positively charged oxygen vacancies may indirectly contribute the development of interface charge accumulation, in addition to directly contributing to oxide charge accumulation in ionization damage. It was shown that a puckered $4\times$ or dimer configuration may react with a hydrogen molecule to produce a proton that may depassivate the interface defects saturated by hydrogen.[12] The activation energy and the reaction energy of the proton-release reaction involving a puckered configuration is 1.23 eV and -0.05 eV, respectively, and those involving a dimer is 0.58 eV and 0.76 eV, respectively. It should be noted that protons should be generated by the reaction involving a puckered configuration in normal devices, because the dimer configuration is unstable according to its thermodynamic charge-state transition level.

Although oxygen vacancy defects have been investigated intensively, the strain effect on their structures, properties, and reactions correlated with ionization damage and more specifically ELDRS is rarely reported. In this work, the strain effect is investigated using *ab-initio* calculations. We find that strain may induce structural relaxations that can partly convert the dimer and unpuckered configurations into the puckered one, and it may influence the relaxation of the puckered configuration after electron recombination and consequently induce more thermodynamic charge-state transition levels in Si band gap. It follows that strain may facilitate the development of both oxide and interface charge accumulations and then enhance ionization damage.

2. Approach

2.1. Classical molecular dynamics simulation

The melting-and-quenching process of silica is simulated to generate the a-SiO_2 model using classical molecular dynamics (MD) implemented by the open-source large-scale atomic/molecular massively parallel simulator (LAMMPS) code.[13,14] The ReaxFF force field that can accurately reproduce the properties of various silica polymorphs is used in the simulations.[15,16] Periodic boundary condition is applied and the time step is set to be 0.5 fs. The simulation begins with a $3\times3\times3$ supercell of α-cristobalite, a crystalline phase of SiO_2, containing 216 atoms. The model is first equilibrated in an isothermal and isobaric (NPT) ensemble at 300 K and 1 atm for 20 ps using the Berendsen thermostat and barostat,[17] and then heated up to 6000 K and kept melting at that temperature for 1000 ps using an isothermal and isochoric (NVT) ensemble, which is sufficient to remove the memory of the initial crystalline structure. It is then quenched down to 0 K at a rate of 4 K/ps, and finally relaxed in an NPT ensemble at 0 K and 1 atm.

2.2. Density functional theory calculations

The first-principles calculations are performed in the framework of density functional theory (DFT) with the Perdew–Burke–Ernzerhof (PBE) parameterization of generalized-gradient approximation (GGA)[18] exchange-correlation implemented in the Vienna *ab initio* simulation package (VASP).[19] The interactions between valence electrons and ionic cores are described using the projector augmented-wave method (PAW)[20] with a cut-off energy of 520 eV. Because of the large size of the a-SiO_2 model ($a = b = 15.03$ Å, $c = 13.98$ Å), the Brillouin-zone integration is limited to the Γ-point only. The convergence criterion of structural optimization is that the total energy difference is less than 10^{-4} eV. For the electronic structure calculations, the criterion is increased to 10^{-5} eV. In order to describe the unpaired electrons, spin polarization is taken into account in the

calculations. To correct the band gap underestimated by PBE-GGA exchange–correlation, hybrid exchange-correlation is applied in the electronic structure calculations, where Hartree–Fock exchange is mixed into PBE at a weight of 35%.[21]

A neutral oxygen-vacancy (NOV) is constructed by removing an oxygen atom from the defect-free a-SiO_2 model and further optimizing the structure. Then, we remove an electron from the NOV and optimize the structure to obtain the positively charged oxygen-vacancy (PCOV). There is a potential barrier of about 0.38 eV between the positively charged dimer structure and the puckered structure. All the structures obtained by this method are dimer structures.[22,23] Therefore, in order to obtain other positively charged structures, we artificially move a silicon atom in the positively charged dimer through the plane where the three coordinated oxygen atoms are located. Then the structure is optimized to obtain other positively charged structures.[10]

The thermodynamic charge-state transition level is defined as the total energy difference between two charge states of a defect in their own fully relaxed ground structures. An electron is added to the supercell containing the PCOV, and the resulting neutral supercell is relaxed by the structural optimization calculation.

2.3. Applying strain

The tensile strain is applied to the a-SiO_2 models each containing a PCOV along the c-axis ([001] direction) and scanned from 0% to 7% with a step of 1%,[24–26] to analyze the effect of strain on the properties of PCOVs. The strain is measured by $\varepsilon = (c - c_0)c_0^{-1} \times 100\%$, where c and c_0 are the strained and original lattice constants, respectively. For a given value of strain, the lattice constant c is fixed, and the model is relaxed along the a and b axes. The tetrahedral parameter t is defined as $t = (360 - \sum_{i=1,3} \alpha_i)/31.5$, where α_i ($i = 1, 2, 3$) are the three O–Si–O bond angles of the three-fold coordinated silicon atom.[8] This parameter is basically determined by the hybridization of the valence electron orbitals of a three-fold coordinated Si atom, and it is also susceptible to the local distortion.

3. Results and discussion

3.1. Defect-free a-SiO_2 with strain

The cell parameters of the a-SiO_2 model optimized by classical MD simulation are $a = b = 15.03$ Å, $c = 13.98$ Å. There is no coordination defect in the model, i.e., each silicon atom is coordinated by four oxygen atoms and each oxygen atom is coordinated by two silicon atoms. The structural parameters of the defect-free a-SiO_2 model are in agreement well with those given by the experiments and other simulations (Table 1). The density of the model is 2.27 g/cm^3, compared to the values given by other simulations using ReaxFF force field ranging from 1.99 g/cm^3 to 2.27 g/cm^3 with an average of 2.16 g/cm^3.[27] The histograms of the Si–O bond length, and the O–Si–O and Si–O–Si bond angles of the model are plotted in Fig. 1.

Table 1. The structure parameters and standard deviations (in parentheses) of the optimized a-SiO_2 model.

	Density/(g/cm^3)	Bond length/Å	Bond angle/(°)	
		Si–O	O–Si–O	Si–O–Si
Theory	2.28[a]	1.62[a]	108.3[a]	139.8[a]
Experiment	2.20[b]	1.62[b]	109.5[c]	144[c]
This work	2.27	1.636 (0.02)	109.477 (6.12)	142.585 (13.74)

[a]Ref. [13], [b]Ref. [32], [c]Ref. [35].

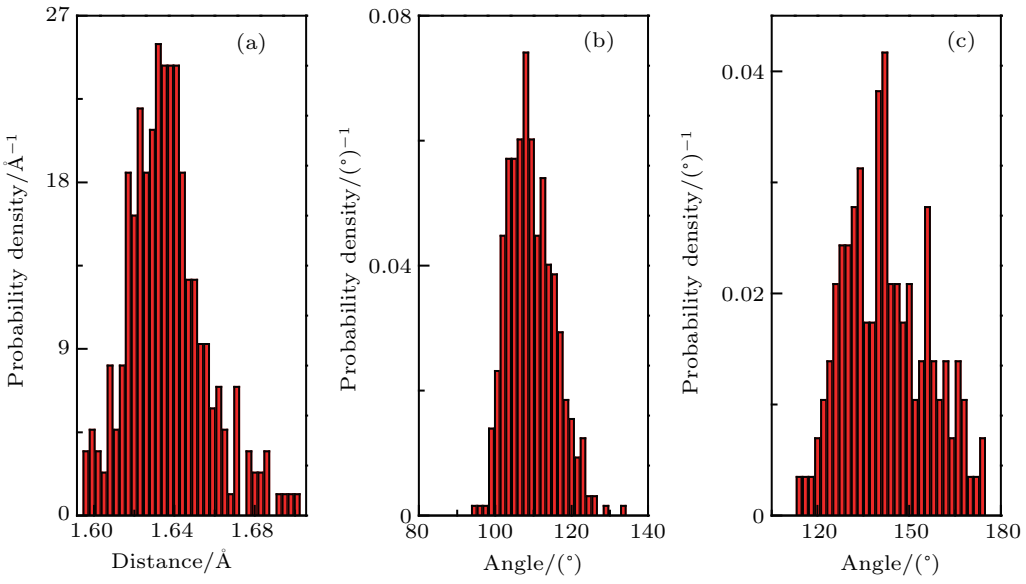


Fig. 1. Histograms of (a) Si–O bond length, (b) O–Si–O bond angle, and (c) Si–O–Si bond angle of the optimized 216-atom a-SiO_2 model.

In addition, ring counting is performed on the model by following Guttman's shortest-path criterion,[28,29] which indicates that the 5-, 6-, and 7-member rings are dominant (Fig. 2(a)), in consistence with the results of the previous studies.[30,31] The radial distribution functions (RDF) are calculated to further exam the structure of the a-SiO_2 model. The inter-atomic distances of Si–O, Si–Si, and O–O nearest-neighbor pairs are identified from the first peaks of the RDFs to be 1.63 Å, 3.15 Å and 2.65 Å (Fig. 2(b)), respectively, close to the experimental values.[32] The band gap calculated with the hybrid exchange correlation is 8.35 eV, close to the experimental value of 9 eV.[33,34]

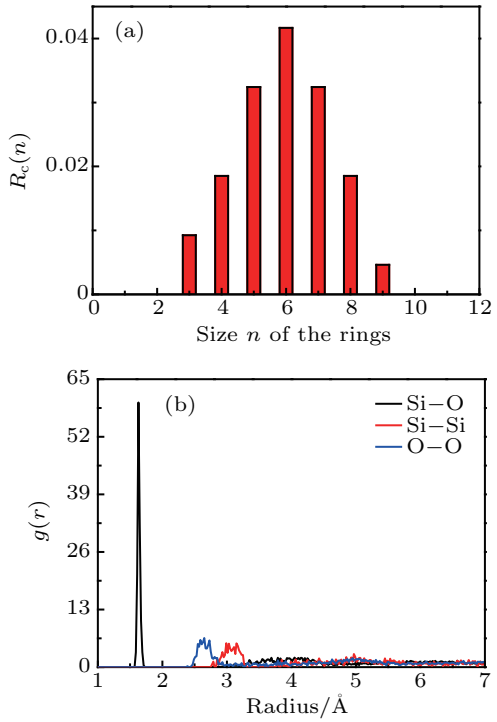


Fig. 2. (a) Ring size distribution by Guttman ring-counting and (b) radial distribution functions of the a-SiO_2 model.

Uniaxial tensile strains ranging from $\varepsilon = 0\%$ to $\varepsilon = 10\%$ are applied along the c-axis of the defect-free a-SiO_2 model. The calculated stress of the model increases linearly with the applied strain (Fig. 3), showing linear elastic behavior.[36] In addition, there is no coordination defect induced by strain. The histograms of the Si–O bond length at the strains of 0%, 3%, and 7% are plotted and compared to each other in Fig. 4(a), where the distribution is shifting toward longer Si–O bond length with increasing the strain. The average Si–O bond length of the non-strained model is 1.636 Å with a standard deviation (std) of 0.02 Å, and increases to 1.644 Å with an std of 0.02 Å at 7% strain. In addition, the strain has an appreciable effect on the distribution of Si–O–Si angle (average of 142.6° under non-strain and 144.1° at 7% strain) but little on the O–Si–O angle (average of 109.5° under non-strain and 7% strain), which is consistent with the conclusion of the previous study on compressive strain.[37] The lattice parameters of the model are plotted versus the tensile strain in Fig. 4(b), where the lattice constants a and b decrease with increasing the strain. The volume of the model increases approximately linearly with the strain as illustrated in the inset of Fig. 4(b). The strain has an influence on the band gap, which decreases by 0.20 eV at 3% strain and by 0.55 eV at 7% strain. Thus, it is possible to adjust the band gap of a-SiO_2 by utilizing the strain induced by lattice or thermal mismatch, which has been reported in silicon.[38]

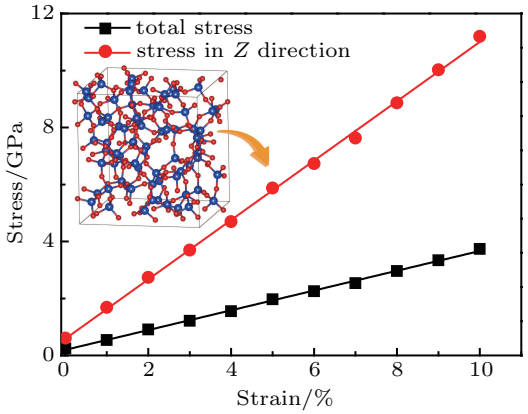


Fig. 3. Calculated stress plotted versus the applied strain to the a-SiO_2 model. The black and red lines represent the total stress and the stress in Z direction, respectively. The a-SiO_2 model is illustrated in the inset.

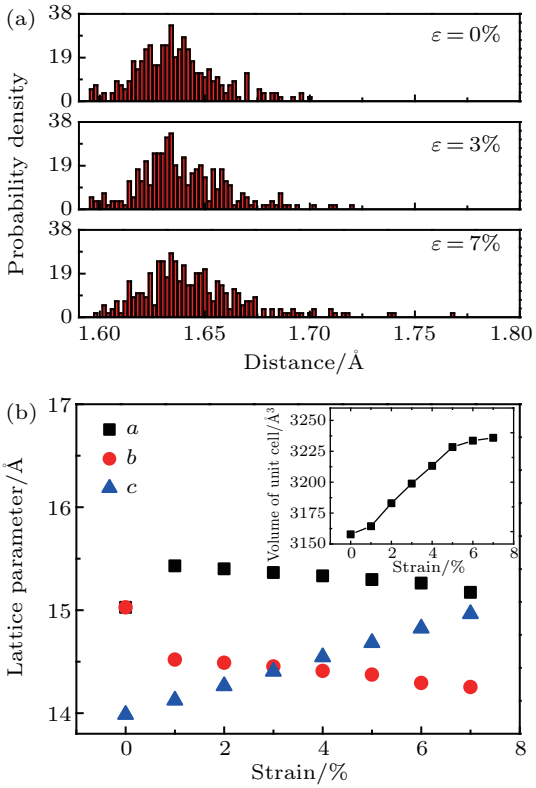


Fig. 4. Calculated (a) histogram of Si–O bond length at different strains and (b) lattice parameters versus the applied strain. Black square, red circle and blue triangle represent lattice constants a, b, and c, respectively. The volume of the model is plotted against the strain in the inset of (b).

3.2. Positively charged oxygen vacancies with no strain

Before investigating the effect of strain on the positively charged oxygen vacancies, we investigate the vacancies in the

non-strained a-SiO_2 model to calibrate the calculations and set up the references.

Sixteen PCOVs in four configurations have been investigated, including 5 positively dimer, 3 unpuckered, 4 puckered four-fold (4×), and 4 puckered five-fold (5×) configurations.[10] The typical structures of the configurations are illustrated in Fig. 5. According to the projection direction of the silicon atom dangling bond (Si-DB), the puckered configurations can be further divided into forward-projected (FP) puckered configurations (the Si-DB points towards the oxygen vacancy center) and back-projected (BP) puckered configurations (the Si-DB points away from the oxygen vacancy center). All the structures are spin-polarized, and the spin density, as shown by the yellow clouds in Fig. 5, is mostly localized on the Si-DB atom and a small part of it on its three oxygen neighbors.

Electron paramagnetic resonance (EPR) is the most powerful approach to probe dangling bond defects in silicon dioxide, by which hyperfine parameters are measured and local structures can be deduced from the parameters. Fermi contact and dipole interaction can be measured in EPR experiments, associated with the isotropic and anisotropy parts of hyperfine tensor, respectively, and proportional to the s- and p-orbital components of a dangling bond, respectively.[39] Fermi contact is generally stronger than dipole interaction for the dangling bonds in a-SiO_2. The calculated Fermi contacts of the PCOVs are listed in Table 2. The calculated Fermi contact of the dimer configurations is −9.6 mT in average with an std of 0.9 mT, close to the experimental value of E'_δ center in a-SiO_2. The average Fermi contacts of the unpuckered, puckered 4× and 5× configurations are close to each other, close to the experimental value of E'_γ center in a-SiO_2.

Table 2. Average Fermi contacts of PCOVs in different configurations that may correspond to different subcategories of E' centers followed by the standard deviations (in parentheses).

Configuration	Structure in Fig. 5	This work/mT	Theory/mT	Experiment/mT
Dimer	(a)	−9.6 (0.9)	−10.7 (1.7)[a]	E'_δ − 10 (1.5)[b]
Unpuckered	(b)	−39.9 (0.4)	−40.3 (2.1)[a]	
Puckered 5×	(c), (d)	−40.5 (3.5)	−41.0 (2.7)[a]	E'_γ − 42 (3)[c]
Puckered 4×	(e), (f)	−41.7 (2.8)	−41.4 (2.3)[a]	

[a]Ref. [22], [b]Ref. [40], [c]Ref. [41].

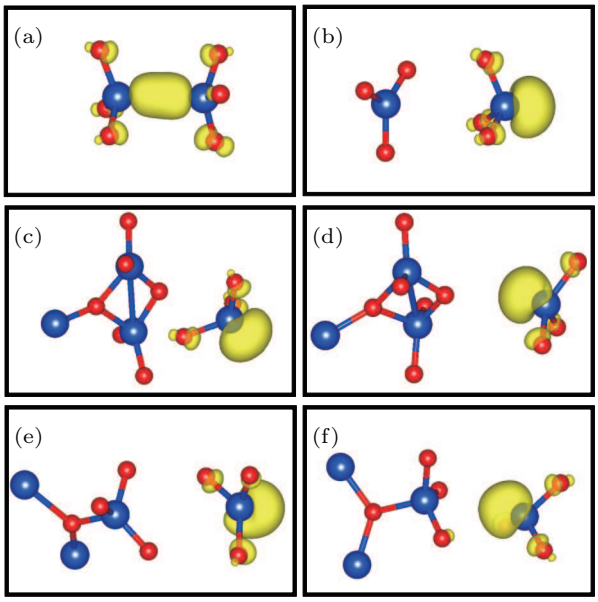


Fig. 5. Typical configurations of PCOVs with spin density, where the isosurface value is set to be 0.01 e/Å^3: (a) dimer, (b) unpuckered, (c) BP 5×, (d) FP 5×, (e) BP 4× and (f) FP 4×. Silicon and oxygen atoms are represented by the big blue and small red balls, respectively, and spin density is rendered as yellow cloud.

3.3. Positively charge oxygen vacancies under strain

3.3.1. Unpuckered configuration

Three samples of unpuckered configuration are created and their typical structure with spin density is illustrated in Fig. 5(b). There are two three-fold coordinated Si atoms in each unpuckered configuration, where one is in sp^2 hybridization ($t = 0$) and the other is in sp^3 hybridization ($t = 1$). After applying tensile strain to the three unpuckered configurations, two of the configurations are transformed into different configurations. The sp^2 hybridized silicon atom in one of the unpuckered configurations moves backward under the strain, and develops a bond with a background oxygen atom, which results in a BP puckered 4× configuration, as shown in Fig. 6(b). The relative total energy of the unpuckered configuration is plotted against the strain (the blue line and round symbols in Fig. 7). It increases with increasing the strain from 1% to 7%, and decreases from 0% to 1% because of the structural transition from the unpuckered configuration at 0% to the BP puckered 4× configuration at 1% (the point I in Fig. 7). The strength of Fermi contact increases from −39.91 mT of the unpuckered configuration at 0% strain to −43.99 mT of the BP puckered 4× configuration at 1% strain, and further increases to −45.37 mT at 7% strain. The defect states of the unpuckered configuration are depicted at the strains of 0%, 3%, and 7%, respectively, as a part of the total density of states (Fig. 8(a)). There is an occupied defect state at 2.32 eV in the spin-up channel and an unoccupied state at 7.24 eV in the spin-down channel at 0% strain, with respect to the valence band maximum (VBM) of the a-SiO_2 model. Applying the strain from 0% to 3% introduces an appreciable shift of the occupied defect state toward higher energy, which is associated with the structural transition. Otherwise, applying the strain from 3% to 7% induces a slight shift of the defect state. The

BP puckered 4× configuration converted from the unpuckered configuration by the strain can retain its structure after capturing an electron (Fig. 6(b)–6(c)). It is shown by Bader charge analysis that the valence electron number on the Si_{a2} atom increases from 1.59 |e|to 2.23 |e|. This indicates that the electron is trapped on the dangling bond Si atom (the Si_{a2} atom in Fig. 6(c)) and paired with the single electron. The puckered moiety keeps positively charged. The total magnetic moment of the BP puckered 4× configuration is zero after capturing an electron.

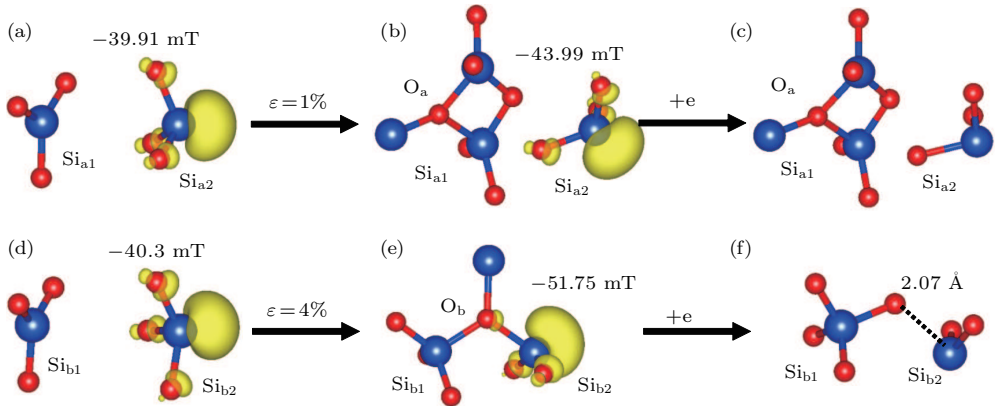


Fig. 6. Strain-induced structural transition from (a), (d) positively charged unpuckered configurations to (b) a BP puckered 4× configuration under 1% strain or (e) a positively charged FO configuration under 4% strain, and structural relaxation induced by electron recombination into (c) neutral BP puckered 4× configuration or (f) a divalent silicon structure.

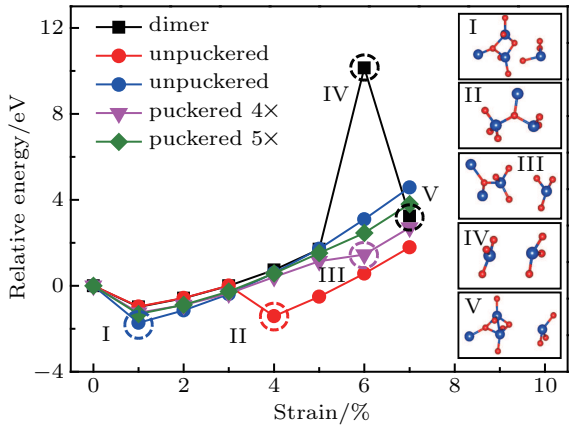


Fig. 7. Relative total energies of PCOVs in different configurations versus strain. The strain-induced structural transitions are circled on the lines and the associated structures are illustrated in the insets.

In addition, another one of the three unpuckered configurations is converted into a forward-oriented (FO) configuration by applying the tensile strain, where the sp^2 hybridized silicon atom in the unpuckered configuration moves forward and develops a covalent bond with one of the three oxygen atoms bonded with the dangling bond Si atom (Si_{b2}), as shown in Fig. 6(e). The relative total energy of this unpuckered configuration is plotted against the applied strain (the red line and round symbols in Fig. 7), where the energy dips to the minimum at 4% strain (the point II in Fig. 7), associated with the structural transition from the unpuckered configuration to the FO configuration. The Fermi contact of the FO configuration is −51.75 mT, close to the experimental value of E'_α center (−49 mT).[41] After capturing an electron, one of the three Si_{b2}–O distance increases by 0.29 Å to 2.07 Å, indicating that the Si_{b2}–O bond is ruptured, and the configuration collapsing into a structure containing a divalent silicon atom (Figs. 6(e)–6(f)).[10,42,43] The Bader charge analysis shows that the electron is trapped by the Si_{b2} atom, and the valence electron number of the Si_{b2} atom increases from 1.63|e| to 2.33|e|. As shown in Fig. 8(b), the occupied defect state of this unpuckered configuration are slightly shifted by increasing the strain from 0% to 3%, and pushed down in energy by 1.31 eV when the strain increases to 7%.

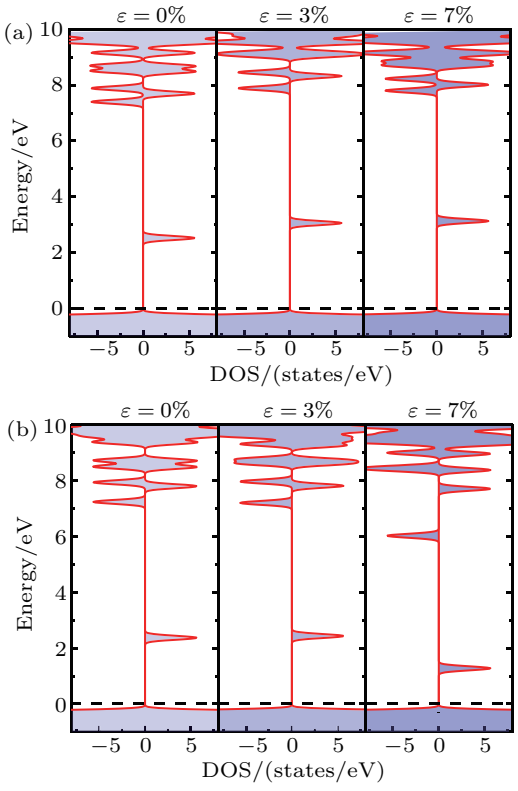


Fig. 8. Evolution of defect states in the transition driven by strain from the unpuckered configuration to (a) the puckered 4× configuration or (b) the FO configuration.

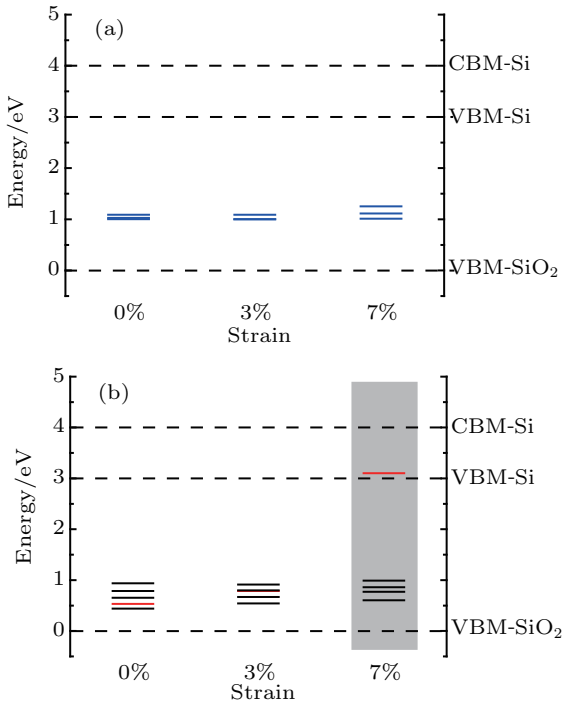


Fig. 9. Thermodynamic charge-state transition levels of (a) three unpuckered configurations (blue short lines) and (b) five dimer configurations (black and red short lines) at 0%, 3%, and 7% strains. The red line in (b) identifies the dimer configuration with the relaxation channel influenced by strain.

The calculated transition levels of the three unpuckered configurations are shown in Fig. 9(a), which show little dependence on the strain.

3.3.2. Dimer configuration

After applying tensile strain to the five dimer configurations, two of the configurations are transformed into different configurations. It may induce two consecutive local structure transitions to one instance of the dimer configurations, as implied by the relative total energy versus strain curve (the black line and square symbols in Fig. 7), where the energy drastically increases at 5% strain, reaches the maximum at 6% strain (the point IV in Fig. 7) and suddenly drop back at 7% strain (the point V in Fig. 7). In fact, as the strain increases from 0% strain, the Si–Si dimer is stretched and eventually broken into two three-fold coordinated Si atoms at 6% strain. The resulting configuration is unpuckered, which is characterized of one three-fold coordinated Si atom in planar triangle structure associated with sp^2 hybridization and the other one in tetrahedral structure associated with sp^3 hybridization, as shown in the inset IV of Fig. 7. It should be noted that the dangling bond is projecting toward the vacancy center in the unpuckered structure. Slightly increasing the strain further from 6% to 7% induces another local structure transition from the unpuckered configuration to the puckered configuration, as shown in Fig. 10(b)–10(c), where the Si_{a1} atom moves backward and develops covalent bonds with not only a background O atom but also the Si atom bonded to that O atom (Fig. 10(c)). The resulting configuration is a FP puckered 5× configuration, as the Si_{a1} atom is five-fold coordinated. The notable bond rearrangement leads to the drastic drop of the total energy from 6% to 7% strain in Fig. 7.

The calculated Fermi contact sensitively reflects the stretching of the Si_{a1}-Si_{a2} inter-atomic distance and the consequential structural transitions. The distance is 2.74 Å for the dimer configuration at 0% strain, where the Fermi contact is calculated to be −9.55 mT, associated with the spin density in between the Si_{a1} and Si_{a2} atoms (Fig. 10(a)). It increases to 3.58 Å as the structure has transited to the unpuckered configuration at 6% strain, where the Fermi contact increases in strength to −29.10 mT. This value is weaker than that of E'_γ center in strength, associated with the spin density localizing substantially on the Si_{a2} atom in sp^3 hybridization but notably extending toward the Si_{a1} atom (Fig. 10(b)). The distance further increases to 4.20 Å due to the strain-induced puckering at 7% strain (Fig. 10(c)), where the Fermi contact further increases in strength to −51.36 mT, close to the experimental value of E'_α center. The strong Fermi contact in the puckered configuration may be attributed to the chemical shift induced by the oxygen atom near the spin cloud of the dangling bond. After recombining with an electron, the dangling bond moiety is relaxed into a two-fold coordinated Si structure, but the puckered moiety is maintained (Fig. 10(d)). It is further shown by the Bader charge analysis that the valence electron population on the dangling bond atom (Si_{a2}) changes from $1.6|e|$ to $2.4|e|$, which implies that the electron is captured by the Si_{a2} atom. In fact, the lone electron pairs resulting from the capture on the dangling bond orbital repels the three Si_{a2}–O bonds in the positively charged configuration, and eventually ruptures the longest and weakest one under strain. This result shows that the strain may impact the Si–O bond lengths and consequently the relaxation channels of the configurations. As a remarkable structural relaxation is triggered by the electron recombination, the thermodynamic charge-state transition level of this instance will be much higher than others.

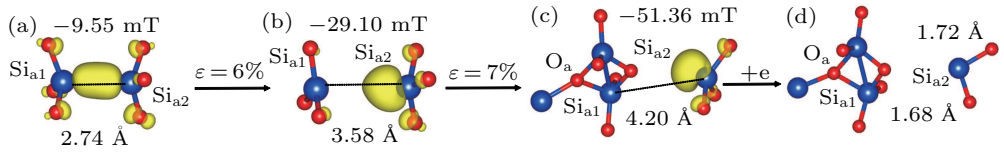


Fig. 10. Strain-induced structural transitions from (a) a positively charged dimer configuration to (b) a unpuckered configuration under 6% strain and the to (c) a FP puckered 5× configuration under 7% strain, and structural relaxation induced by electron recombination into (d) a two-fold coordinated Si structure under 7% strain.

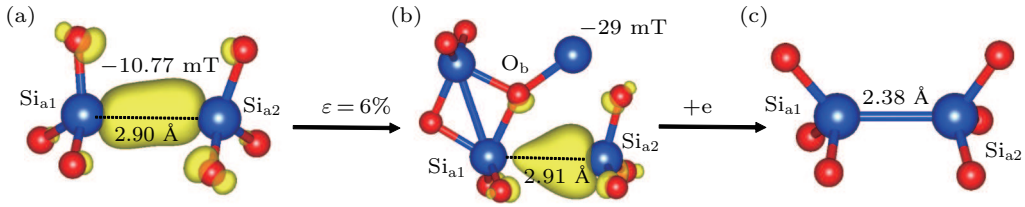


Fig. 11. Strain-induced structural transition from (a) a positively charged dimer configuration to (b) an interim between the dimer configuration and the puckered configuration at 6% strain, and structural relaxation induced by electron recombination into (c) a neutral dimer configuration under 6% strain.

However, another instance of the dimer configurations, characterized by a longer Si_{a1}–Si_{a2} inter-atomic distance of 2.90 Å under no strain, experiences only one local structural transition to an interim between the dimer configuration and the puckered configuration at 6% strain (Fig. 11). In fact, the Si_{a1} atom in the resulting structure is bonded with an O atom and a Si atom in the background besides the three Si–O bonds, forming the five-fold puckered moiety. Moreover, the strain-induced puckering slightly increases the Si_{a1}–Si_{a2} distance to 2.91 Å, which is still within the range of dimer configuration (2.94 Å).[22] The spin density is localized in between the Si_{a1} and Si_{a2} atoms under no strain, and inclined to the Si_{a2} atom after the transition. Accordingly, the calculated Fermi contact is −10.77 mT under no strain, and −29 mT, a value between those of E'_δ and E'_γ centers, after the transition. The Si_{a1}–Si_{a2} distance, the spin density, and the calculated Fermi contact consistently show that the resulting structure is a transitional structure from a dimer configuration to an FP puckered 5× configuration. After capturing an electron, the puckered configuration collapses and reverts to a neutral dimer because of the relatively short Si_{a1}–Si_{a2} distance (Fig. 11(c)).

The thermodynamic charge-state transition levels of the five dimer configurations at the strains of 0%, 3% and 7% are calculated and illustrated in Fig. 9(b). The levels under no strain are distributed from 0.4 eV to 0.9 eV, slightly higher than the VBM of a-SiO_2 and much lower than that of Si. Thus, the dimer configurations will be thermodynamically stable in the neutral charge state, assuming that the Fermi level is at the middle of the Si band gap in regular devices. However, there is a thermodynamic charge-state level in Si band gap at about 3 eV with respective to a-SiO_2 VBM under 7% strain (red line in Fig. 9(b)), which is associated with the instance that relaxes into the two-fold coordinated Si structure after capturing an electron. This makes the instance a possible deep hole trap that may contribute to oxide charge accumulation.

The calculated total density of states show that the strain has a remarkable influence on the defect levels of the dimer configurations, especially on those undergoing the structural transitions (Fig. 12). The defect levels, both occupied and unoccupied, move toward the conduction band minimum under the strain. For the dimer configuration induced puckered 5× configuration at 7% in Fig. 12(a), the occupied defect level shifts from 0.18 eV no-strain to 1.63 eV at 3% strain to 2.73 eV at 7% strain, with respective to the VBM. The occupied defect level of another dimer structure shifts by 1.15 eV when the strain increased from 0% strain to 7% (Fig. 12(b)). The reason is that the dimer is converted into an interim between the dimer configuration and the puckered configuration at 6% strain.

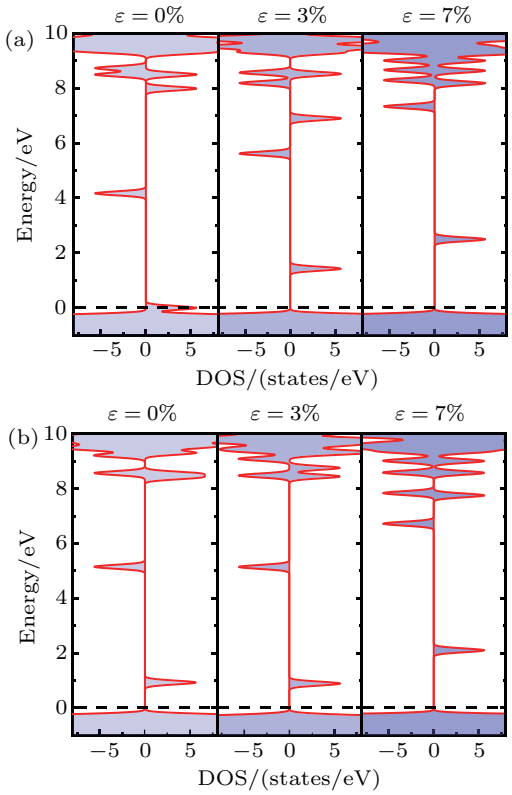


Fig. 12. Evolution of the defect levels under strain: (a) the dimer configuration with the transition to a puckered 5× configuration at 7% strain, and (b) the dimer configuration with the transition to an interim between the dimer configuration and the puckered configuration at 6% strain.

3.3.3. Puckered 4× and 5× configurations of E' center under strain

Uniaxial tensile strain is applied to four puckered 4× configurations in the range of 0%–7%. As the strain increases, the Si–Si distance in one FP configurations gradually increases, and the dangling bond Si atom (Si_{a2}) moves across the plane of the three oxygen atoms bonding to it, becoming a BP configuration (Fig. 13(b)). In addition, the average distance of the Si_{a2}–O bonds increases from 1.67 Å to 1.70 Å. As illustrated in Fig. 7 (the magenta line and triangle symbols), the relative total energy of the puckered 4× configuration smoothly increases with the strain increasing, except the dip at 6% strain

associated with the transition from FP to BP. The Fermi contact of the Si_{DB} atom is enhanced by the back oxygen atom in the BP configuration from −39.47 mT to −52.6 mT, which is close to the experimental value of E'_α center.

In the four puckered 4× configurations investigated in this work, two FP puckered 4× configurations become neutral dimer configurations and two BP puckered 4× configurations maintain the puckered configurations after capturing electrons under no strain. The relaxation channel of the BP puckered 4× configurations after capturing an electron is impacted by the strain. The dangling bond moiety of the BP puckered 4× configuration is maintained after capturing an electron under no strain. It, however, relaxes into a two-fold coordinated Si structure at 6% strain, as shown in the inset of Fig. 13(c). It is shown by the Bader charge analysis that the valence electron population of the Si_{a2} increases by $0.8|e|$ to $2.4|e|$ at 6% strain. This implies that the electron is trapped by the Si_{a2} atom. As shown in the inset of Fig. 13(c), the longest one Si_{a2}–O bond is ruptured after the electron-trapping, leading to a two-fold coordinated Si structure, and the puckered moiety is maintained.

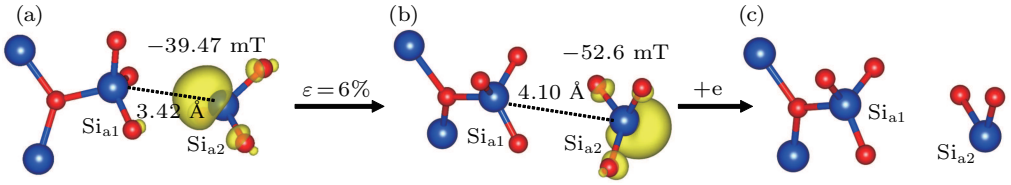


Fig. 13. Strain-induced structural transition from (a) a positively charged FP puckered 4× configuration to (b) a BP puckered configuration under 6% strain, and structural relaxation induced by electron recombination into (c) a two-fold coordinated Si structure under 6% strain.

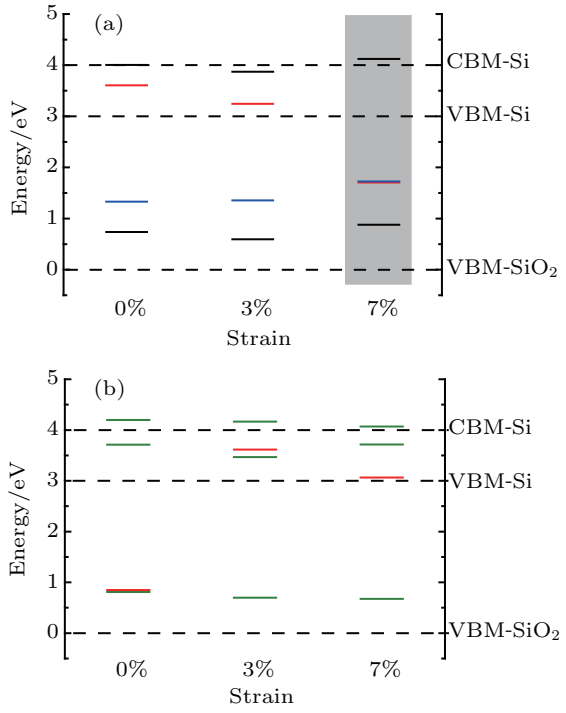


Fig. 14. Thermodynamic charge-state transition levels of (a) the four puckered 4× configurations (black and red short lines) and (b) the four puckered 5× configurations (green and red short lines) under the strains of 0%, 3%, and 7%. The red and blue lines in (a) and (b) represent the puckered 4× and 5× configurations with the relaxation channels influenced by strain. One blue line and one red line in (a) coincide at 7% strain at 1.70 eV.

The thermodynamic charge-state transition levels of the four puckered 4× configurations are distributing in a wide range (Fig. 14(a)), because the neutral structures can be dimer structure, puckered 4× structure, or two-fold coordinated Si structure. There are two instances that maintain the puckered 4× structure after capturing an electron, whose thermodynamic charge-state transition levels are higher than Si VBM. The other instances capture an electron and collapse into a neutral dimer structure, whose thermodynamic charge-state transition levels are higher than a-SiO_2 VBM. Due to the influence of strain, two 4× structures capture electrons and form a two-fold coordinated Si structure, whose thermodynamic charge-state transition levels coincide at 1.70 eV in Fig. 14(a) with respective to the a-SiO_2 VBM.

The calculations on four positively charged puckered 5× configurations show that they are inert to strain. The total energy of the configuration smoothly increases with the strain (the olive line and diamond symbols in Fig. 7). There is no structural transition in the range of 0%–7% strain. In the four puckered 5× configurations investigated in this work, two FP configurations relax into neutral dimer configurations and two BP configurations maintain the puckered configurations after capturing electrons under no strain. There is one FP configuration that collapses into a neutral dimer structure after capturing an electron under no strain (red line in Fig. 14(b)). However, it can maintain the puckered configuration under strain, whose thermodynamic charge-state transition levels are higher than Si VBM (red line in Fig. 14(b)). Since the puckered 4× and 5× configurations do not undergo structural transitions, their defect levels do not move significantly.

4. Conclusions

Using *ab-initio* calculations based on DFT, we have systematically studied the influences of strain on the positively charged oxygen vacancy defects in a-SiO_2. The calculations of relative total energy show that the total energy increases with the strain, and that when there is a structural transition, the total energy can be significantly fluctuated. It has been found that the Si–O bonds in the configurations can be activated by strain. The dimer and unpuckered configurations are sensitive to strain, and may experience a structural transition.

The dimer configuration may relax into a puckered 5× configuration under strain, and the unpuckered configuration may relax into a puckered 4× configuration or an FO configuration. The tensile strain influences the orientation of dangling bond in the puckered 4× configurations, and converts the FP orientation into the BP orientation. The calculations show that the puckered 5× is the most inert to the strain. Moreover, the strain-induced structural transition is irreversible. This implies that the resulting configurations, namely puckered 5×, puckered 4× and FO, may increase in concentration under strain. In addition, the Fermi contacts of the puckered 4× and 5× configurations under the strain are close to the experimental value of E'_α center, which may enrich the microstructure of E'_α center.

The study of defect levels shows that the transition of defect structure introduces an appreciable shift of the occupied defect state. Driven by the strain, an unpuckered configuration is converted into a puckered 4× configuration, and the defect level moves to higher energy, and another is converted into an FO configuration, and the defect level moves to lower energy. The defect levels, both occupied and unoccupied of dimer configuration undergoing the structural transitions, move toward the conduction band minimum under the strain. Since the puckered 4× and 5× configurations do not undergo structural transitions, their defect levels do not move significantly. There is a thermodynamic charge-state transition level of one dimer configuration in Si band gap at about 3 eV with respective to a-SiO_2 VBM under 7% strain, which is associated with the instance that relaxes into the two-fold coordinated Si structure after capturing an electron. The thermodynamic charge-state transition levels of the puckered 4× and puckered 5× configurations are distributing in a wide range. Driven by the strain, two puckered 4× configurations cannot keep the puckered structure unchanged or collapse into a dimer structure after capturing an electron but relax into a two-fold coordinated Si structure with the puckered moiety maintained, whose thermodynamic charge-state transition levels are higher than a-SiO_2 VBM. One FP puckered 5× configuration collapses into neutral dimer structure after capturing an electron under no-strain. However, it can keep the neutral 5× structure unchanged by applying strain, whose thermodynamic charge-state transition levels are higher than Si VBM. This work can help to explore performance degeneration of silicon devices under strain from a microscopic point of view. We call for an EPR study on irradiated a-SiO_2 under strain.

References

[1] Schwank J R, Shaneyfelt M R, Fleetwood D M, Felix J A, Dodd P E, Paillet P and Ferlet-Cavrois V 2008 *IEEE Trans. Nucl. Sci.* **55** 1833

[2] Johnston A H, Swimm R T and Miyahira T F 2010 *IEEE Trans. Nucl. Sci.* **57** 3279

[3] Witczak S C, Lacoe R C, Osborn J V, Hutson J M and Moss S C 2005 *IEEE Trans. Nucl. Sci.* **52** 2602

[4] Enlow E W, Pease R L, Combs W, Schrimpf R D and Nowlin R N 1991 *IEEE Trans. Nucl. Sci.* **38** 1342

[5] Shaneyfelt M R, Pease R L, Schwank J R, Maher M C, Hash G L, Fleetwood D M, Dodd P E, Reber C A, Witczak S C, Riewe L C, Hjalmarson H P, Banks J C, Doyle B L and Knapp J A 2002 *IEEE Trans. Nucl. Sci.* **49** 3171

[6] Boch J, Fleetwood D M, Schrimpf R D, Cizmarik R R and Saigne F 2003 *IEEE Trans. Nucl. Sci.* **50** 2335

[7] Shaneyfelt M R, Pease R L, Maher M C, Schwank J R, Gupta S, Dodd P E and Riewe L C 2003 *IEEE Trans. Nucl. Sci.* **50** 1784

[8] Blöchl P E 2000 *Phys. Rev. B* **62** 6158

[9] Yue Y, Song Y and Zuo X 2018 *Chin. Phys. B* **27** 037102

[10] Uchino T and Yoko T 2006 *Phys. Rev. B* **74**

[11] Lu Z Y, Nicklaw C J, Fleetwood D M, Schrimpf R D and Pantelides S T 2002 *Phys. Rev. Lett.* **89** 285505

[12] Yue Y, Li P, Song Y and Zuo X 2018 *J. Non-Cryst. Solids* **486** 1

[13] Sheikholeslam S A, Manzano H, Grecu C and Ivanov A 2016 *J. Mater. Chem. C* **4** 8104

[14] Plimpton S 1995 *J. Comput. Phys.* **117** 1

[15] Fogarty J C, Aktulga H M, Grama A Y, van Duin A C and Pandit S A 2010 *J. Chem. Phys.* **132** 174704

[16] van Duin A C T, Dasgupta S, Lorant F and Goddard W A 2001 *J. Phys. Chem. A* **105** 9396

[17] Berendsen H J C, Postma J P M, van Gunsteren W F, DiNola A and Haak J R 1984 *J. Phys. Chem.* **81** 3684

[18] Perdew J P, Burke K and Ernzerhof M 1996 *Phys. Rev. Lett.* **77** 3865

[19] Kresse G and Furthmüller J 1996 *Phys. Rev. B* **54** 11169

[20] Kresse G and Joubert D 1999 *Phys. Rev. B* **59** 1758

[21] Alkauskas A, Broqvist P, Devynck F and Pasquarello A 2008 *Phys. Rev. Lett.* **101** 106802

[22] Giacomazzi L, Martin-Samos L, Boukenter A, Ouerdane Y, Girard S and Richard N 2014 *Phys. Rev. B* **90**

[23] Stirling A, Pasquarello A, Charlier J and Car R 2000 *Phys. Rev. Lett.* **85** 2773

[24] Al-Shami A, Lakhal M, Hamedoun M, El Kenz A, Benyoussef A, Loulidi M, Ennaoui A and Mounkachi O 2018 *Sol. Energy Mater. Sol. Cells* **180** 266

[25] Grote C and Berger R F 2015 *J. Phys. Chem. C* **119** 22832

[26] Zhou W, Liu Y, Yang Y and Wu P 2014 *J. Phys. Chem. C* **118** 6448

[27] El-Sayed A M, Watkins M B, Grasser T, Afanas'ev V V and Shluger A L 2015 *Phys. Rev. Lett.* **114** 115503

[28] Le Roux S and Petkov V 2010 *J. Appl. Crystallogr.* **43** 181

[29] Guttman L 1990 *J. Non-Cryst. Solids* **116** 145

[30] Trachenko K and Dove M T 2003 *Phys. Rev. B* **67**

[31] Rino J P, Ebbsjö I, Kalia R K, Nakano A and Vashishta P 1993 *Phys. Rev. B* **47** 3053

[32] Mozzi R L and Warren B E 1969 *J. Appl. Crystallogr.* **2** 164

[33] Grunthaner F J and Grunthaner P J 1986 *Mater. Sci. Rep.* **1** 65

[34] Griscom D L 1977 *J. Non-Cryst. Solids* **24** 155

[35] Dupree E and Pettifer R F 1984 *Nature* **308** 523

[36] Pedone A, Malavasi G, Menziani M C, Segre U and Cormack A N 2008 *Chem. Mater.* **20** 4356

[37] Kuo C L, Lee S and Hwang G S 2008 *Phys. Rev. Lett.* **100** 076104

[38] Wei Q, Zhang Q, Yan H, Zhang M and Zhang J 2018 *Mater. Res. Bull.* **102** 1

[39] Bahramy M S, Sluiter M H F and Kawazoe Y 2006 *Phys. Rev. B* **73**

[40] Stesmans A, Jivanescu M and Afanas'ev V V 2011 *Europhys. Lett.* **93** 16002

[41] Buscarino G, Agnello S and Gelardi F M 2006 *Phys. Rev. Lett.* **97** 135502

[42] Uchino T, Takahashi M and Yoko T 2001 *Phys. Rev. Lett.* **86** 1777

[43] Donadio D, Bernasconi M and Boero M 2001 *Phys. Rev. Lett.* **87** 195504